CrystEngComm

Precise control of density and strength of acid sites of MFI-type zeolite nanoparticles via simultaneous isomorphous substitution by Al and Fe

Journal:	*CrystEngComm*
Manuscript ID	CE-ART-07-2020-001031.R1
Article Type:	Paper
Date Submitted by the Author:	28-Aug-2020
Complete List of Authors:	Yabushita, Mizuho; Tohoku University, Institute of Multidisciplinary Research for Advanced Materials Kobayashi, Hiroki; Tohoku University, Institute of Multidisciplinary Research for Advanced Materials Neya, Atsushi; Tohoku University, Institute of Multidisciplinary Research for Advanced Materials Nakaya, Masafumi; Tohoku University, Institute of Multidisciplinary Research for Advanced Materials Maki, Sachiko; Tohoku University, Institute of Multidisciplinary Research for Advanced Materials Matsubara, Masaki; Tohoku University, Institute of Multidisciplinary Research for Advanced Materials; Sendai National College of Technology - Natori Campus Kanie, Kiyoshi; Tohoku University, Institute of Multidisciplinary Research for Advanced Materials Muramatsu, Atsushi; Tohoku University, Institute of Multidisciplinary Research for Advanced Materials; Japan Science and Technology Agency, Core Research for Evolutional Science and Technology

ARTICLE

Precise control of density and strength of acid sites of MFI-type zeolite nanoparticles via simultaneous isomorphous substitution by Al and Fe†

Received 00th January 20xx,
Accepted 00th January 20xx

DOI: 10.1039/x0xx00000x

Mizuho Yabushita,*‡[a] Hiroki Kobayashi,[a] Atsushi Neya,[a] Masafumi Nakaya,[a] Sachiko Maki,[a] Masaki Matsubara,[a,b] Kiyoshi Kanie[a] and Atsushi Muramatsu*[a,c]

MFI-type zeolite nanoparticles substituted isomorphously by both Al and Fe and of crystallite size ≤51 nm were prepared via a hydrothermal synthesis method combined with a pre-heating treatment. Quantitative assessment of the density and strength of acid sites of the synthesized MFI-type zeolites using temperature-programmed desorption of NH_3 demonstrated that the strength and density of the acid sites on the synthesized zeolites were linearly dependent on the contents and relative ratios of Al and Fe, and the acidities of the [Al, Fe]-MFI-type zeolites were between those of [Al]-MFI and [Fe]-MFI. The observed direct correlations also indicated that the density and strength of acid sites of the MFI-type zeolites were tunable by simply altering the relative amounts of reagents used. Such controlled and moderate acidity for the [Al, Fe]-MFI-type nanoparticles facilitated the suppression of coke formation in the catalytic conversion of dimethyl ether to light olefins.

Introduction

Zeolites, porous and crystalline silicates that typically contain a variety of heteroatoms in a three-dimensional framework, have been recognized as attractive functional materials and have been widely employed as solid acid catalysts in industrial chemical processes such as cracking and upgrading of oils,[1–10] along with other types of porous materials including mesoporous materials for various catalytic reactions and drug delivery systems.[11–13] The acidic properties of zeolites, particularly their density and strength, are of great importance for catalytic performance[1–10] and thus need to be adjusted carefully when targeting specific reactions. This is exemplified by the production of light olefins from methanol (so-called methanol-to-olefins (MTO) reaction) and dimethyl ether (DME)-to-olefins (DTO reaction), where strong acid sites on the solid surface exhibit excellent reaction rates at the beginning of the reaction, but then readily undergo deactivation due to severe coke deposition; thus, acid sites of moderate strength which offer both high product selectivity and prolonged catalyst lifetime are favored.[14–17] Isomorphous substitution of Si^{4+} by trivalent cations is responsible for the formation of Brønsted acid sites on a zeolite surface and acidity of such sites is dependent on a class of the incorporated elements; for example, the Brønsted acidity of Al-incorporated MFI (denoted as [Al]-MFI) is stronger than that of the Fe-substituted one ([Fe]-MFI).[18,19] Although the acid-site density is tunable upon an increase/decrease of the heteroatom content in the zeolite framework, a simple alteration of a class of heteroatom only leads to a discrete change of average acidity. On the other hand, simultaneous incorporation of two different heteroatoms into the zeolite framework may be a possible approach to achieving wide-ranging control of the acidic and catalytic properties; indeed, the combinations of Al and B as well as Al and Fe have been reported to enhance the catalytic performance of MFI-type zeolites, compared to the MFI zeolite substituted by Al solely.[20–22] In this regard, we hypothesize that the average acidity of the MFI zeolite is continuously and precisely controlled between the maximum and minimum average acidity given by [Al]-MFI and [Fe]-MFI, respectively, by changing the contents of Al and Fe as well as the relative molar ratios.

From the perspective of efficient use of the acid sites, which are present mainly on the internal surfaces of zeolites, small particle sizes are highly desirable, given the fact that a short diffusion path length in the catalyst particles allows substrate molecules to gain ready access to the acid sites.[7,23,24] To the best of our knowledge, although such size-controlled

[a] *Institute of Multidisciplinary Research for Advanced Materials, Tohoku University, 2-1-1 Katahira, Aoba-ku, Sendai, Miyagi 980-8577, Japan. E-mails: m.yabushita@tohoku.ac.jp (M.Y.) and mura@tohoku.ac.jp (A.M.)*
[b] *National Institute of Technology, Sendai College, 48 Nodayama, Medeshima-Shiote, Natori, Miyagi 981-1239, Japan*
[c] *Core Research for Evolutional Science and Technology, Japan Science and Technology Agency, 4-1-8 Honcho, Kawaguchi, Saitama 332-0012, Japan*
†Electronic supplementary information (ESI) available: N_2 physisorption isotherms, parametric plot of external surface area as a function of the crystallite size, ^{27}Al MAS NMR spectra, NH_3-TPD profiles, parametric plot of ΔH_{NH3} for a physical mixture of A50F0 and A0F50, DRIFT spectra, detailed results of each DTO reaction, differences of catalyst lifetime in the DTO reaction between [Al, Fe]-MFI and a physical mixture of A50F0 and A0F50, and data of recycle test of A200F50. See DOI: 10.1039/x0xx00000x
‡*Present address: Department of Applied Chemistry, School of Engineering, Tohoku University, Aoba 6-6-07, Aramaki, Aoba-ku, Sendai, Miyagi 980-8579, Japan.*

synthesis of zeolites containing a single heteroatom has been studied intensively,[25] zeolite nanoparticles isomorphously substituted with multiple heteroatoms over a wide range of compositions have yet to be synthesized; in other words, simultaneous control of the acidic properties of zeolite nanoparticles by introducing multiple heteroatoms as well as control of the particle size are attractive but still remain a challenge in the field of zeolite chemistry.

In our previous report, it was reported that heat-treatment at 70 °C with pH control using HCl prior to hydrothermal treatment was effective for reducing the particle size of the resulting [Fe]-MFI zeolites.[26] Here, in this study, the preparation of MFI-type zeolite nanoparticles containing both Al and Fe in the same framework using the aforementioned pre-heating technique is addressed and it is demonstrated that the density and strength of the acid sites were linearly controlled by simply altering the contents and relative ratios of Al and Fe. The synthesized zeolite nanoparticles were then employed in the DTO reaction to investigate the effects of precise control of the density and strength of acid sites of the nanoparticles on catalytic performance.

Experimental section

Hydrothermal synthesis of MFI-type zeolite nanoparticles

All reagents were purchased from FUJIFILM Wako Pure Chemical and Tokyo Chemical Industry and used as received. MFI-type zeolite nanoparticles containing either or both Al and Fe atoms were synthesized by following a previously reported hydrothermal synthesis method for [Fe]-MFI.[26] Thus, an aqueous solution of either or both $Al(NO_3)_3$ and $Fe(NO_3)_3$ was prepared, and a 40 wt% tetrapropylammonium hydroxide (TPAOH) aqueous solution was added in a dropwise manner; thereafter, the resulting solution was stirred at room temperature for 10 min. In the case of synthesis of [Al]-MFI with a Si/Al molar ratio of ≤100, NaCl was also dissolved in the solution. After the addition of 2.0 M HCl aqueous solution, the solution was stirred for a further 10 min. Then, tetraethyl orthosilicate (TEOS) was added, and the mixture was stirred initially at 0 °C for 6 h not to cause the hydrolysis of TEOS and subsequently at room temperature for 42 h. Note that the molar ratios of $TEOS/Al(NO_3)_3/Fe(NO_3)_3/TPAOH/HCl/NaCl/H_2O$ were adjusted to 1.0/0–0.02/0–0.02/0.5/0.1–0.2/0–0.06/30. The solution was then transferred to a Teflon-lined high-pressure reactor (Parr Instrument Company, inner volume 100 mL), pre-heated at 70 °C for 24 h, and then heated at 160 °C for 2–7 days. The solid phase was washed using a centrifuge five times with deionized water. After drying at 60 °C and calcination in air at 540 °C for 12 h, the MFI-type zeolite with Na^+ counter cations was obtained. Afterwards, the resulting powder was treated four times in 1 M NH_4Cl aqueous solution at 60 °C for 1 h. After washing 10 times using the centrifuge and drying at 60 °C for 24 h, the resulting material was calcined in air at 540 °C for 12 h to obtain the MFI-type zeolite with H^+ counter cations. The prepared zeolites are denoted hereafter as AXFY, where X and Y represent the Si/Al and Si/Fe ratios, respectively, based on the relative amounts of reagents used.

Characterization of zeolites

The crystal structure of each sample was identified by powder X-ray diffraction measurement (XRD; Ultima IV, Rigaku, equipped with a semiconductor detector, Cu Kα radiation (40 kV, 40 mA)). The morphology of the zeolite particles was investigated using field-emission scanning electron microscopy (FE-SEM; S-4800, Hitachi High-Tech) after sputter coating with Pt (thickness of *ca.* 10 nm). The porous structure was assessed by N_2 physisorption measurement (BELSORP-mini, MicrotracBEL, –196 °C), after pretreatment at 400 °C for 2 h under N_2 flow (50 mL min^{-1}). The actual contents of Al and Fe in the zeolite samples were determined by X-ray fluorescence spectroscopy (XRF; ZSX Primus II, Rigaku). The coordination states of Al and Fe were elucidated using solid-state ^{27}Al magic angle spinning nuclear magnetic resonance spectroscopy (^{27}Al MAS NMR; AVANCE III 600, Bruker, ^{27}Al 156 MHz, MAS frequency 15 kHz) and diffuse reflectance ultraviolet-visible spectroscopy (DR-UV-vis; H-3900, Hitachi, each sample was diluted with $BaSO_4$), respectively. The density and average strength of acid sites were examined via NH_3 temperature-programmed desorption (NH_3-TPD; BELCAT, MicrotracBEL, equipped with a quadrupole mass spectrometer (Q-MS; BELMass, MicrotracBEL), temperature range 100–700 °C, ramp rate 10 °C min^{-1}) and using a previously reported method to estimate the enthalpy change upon NH_3 desorption.[27] Prior to the measurement, acid sites on the sample surface were saturated with NH_3 at 100 °C, and then the weakly-adsorbed NH_3 species were removed via water vapor treatment (100 °C, partial pressure 4 kPa, 30 min).[28] Acidic OH groups in the zeolite samples were characterized by diffuse reflectance infrared Fourier transform spectroscopy (DRIFT; FTS 7000, Digilab) after pretreatment at 450 °C for 1 h under Ar flow (50 mL min^{-1}).

Catalytic conversion of dimethyl ether to light olefins

The catalytic performance of the synthesized zeolites for the DTO reaction was examined using a fixed-bed flow reactor. In each reaction, 200 mg of catalyst in granular form (diameter 355–500 μm) was mixed with 840 mg of quartz sand (diameter 600–850 μm) and charged into a quartz tube (inner diameter 7 mm), which was then placed in an electric furnace. The catalyst was pre-treated at 550 °C for 1 h under air flow (60 mL min^{-1}) and subsequently at the same temperature for 1 h under Ar flow (60 mL min^{-1}). DME was continuously flowed through the catalyst bed at 450 °C with a contact time (W/F) of 5.8 g h mol^{-1}. The outlet gas containing C_2–C_4 olefins was directly analyzed by an on-line gas chromatograph (GC; GC 8A, Shimadzu) equipped with a flame ionization detector (FID) in conjunction with a Gaskuropack 54 packed column (GL Sciences). The amount of coke deposited on the catalyst surface was quantified by thermogravimetric analysis (TGA; SII TG/DTA 7200, Hitachi High-Tech, ramp rate 10 °C min^{-1}), where the quantity of coke formed on the catalyst surface was

ARTICLE

Table 1 Textural properties of the synthesized MFI zeolites

Sample	Molar ratio of synthesis gel		Molar ratio of synthesized zeolite[a]		D^b /nm	$V_{cell}{}^c$ /Å^3	$S_{BET}{}^d$ /m^2 g^{-1}	$S_{external}{}^e$ /m^2 g^{-1}
	Si/Al	Si/Fe	Si/Al	Si/Fe				
A50F0	50	–	50	–	44	5375	440	48
A100F0	100	–	97	–	46	5370	450	51
A200F0	200	–	200	–	51	5350	490	47
A400F0	400	–	400	–	48	5344	480	39
A0F50	–	50	–	51	29	5366	490	87
A0F100	–	100	–	100	43	5356	510	64
A50F50	50	50	58	57	35	5392	490	74
A100F50	100	50	110	56	31	5381	510	73
A200F50	200	50	220	55	33	5376	480	66
A400F50	400	50	440	55	29	5375	490	100
A800F50	800	50	810	55	28	5375	500	110
A100F100	100	100	97	99	36	5367	490	57
A150F75	150	75	150	74	36	5374	500	73
A300F150	300	150	290	150	31	5361	500	85

[a] Quantified by XRF measurement. [b] Crystallite size, determined by applying the Scherrer equation to the 011 reflection at 2θ of 7.9°,[29] due to the overlap of the most prominent peak observed at 2θ of 23.1° with other peaks. [c] Unit cell volume, calculated from the XRD patterns. [d] BET specific surface area. [e] External surface area, estimated via the *t*-plot method.

defined as the weight difference of the used catalyst between 300 °C and 800 °C.

The catalyst recycle test was also conducted as follows. Thus, after each run, the reactor was initially cooled down to room temperature, and then the temperature was increased to 550 °C with a ramp rate of 5 °C min^{-1} and maintained for 6 h under air flow (60 mL min^{-1}), in order to remove coke and organic compounds deposited on the catalyst surface. After the reactor was again cooled down to room temperature, the next run was started.

Results and discussion

A series of hydrothermally synthesized samples were characterized by various analytical techniques. The molar ratios of Si/Al and Si/Fe for each sample estimated by XRF were almost the same as those values for the corresponding synthesis gels before the hydrothermal treatment (Table 1). If all the sources of Si and heteroatoms used for the hydrothermal synthesis are assumed to have been recovered completely as solid products, the consistency in the data suggests that Al^{3+} and Fe^{3+} ions in the starting reagents were taken into the resulting solid materials; in other words, both the Si/Al and the Si/Fe ratios of the products can be controlled by simply changing the reagent amounts. The XRD patterns in Fig. 1 demonstrated that all samples had the MFI-type framework structure. No diffraction peaks assignable to other oxides (*e.g.*, Al_2O_3, Fe_2O_3, and Fe_3O_4) were observed in any cases. The crystallite sizes calculated by the Scherrer equation were 29–51 nm, the values of which were in agreement with the sizes of the spherical- or cubic-shaped uniform particles observed by FE-SEM (Fig. 2), considering the thickness of the Pt-coating layer (*ca.* 10 nm). These crystallite sizes were smaller than those for previously reported [Al, Fe]-MFI zeolites,[30,31] and the formation of such small crystals was previously achieved only via a planetary ball-milling process as a post-synthetic treatment.[32] As reported elsewhere, these small particles are of great advantage in catalytic reactions, given the fact that substrate molecules can easily access the internal surfaces of zeolite materials due to the short diffusion path lengths toward the acid sites.[7,23,24] Compared to the cases where Al species were solely incorporated into the zeolite framework, a decreasing tendency for the crystallite sizes in the presence of Fe was also observed. This trend implies that Fe species might act as an inhibitor for crystal growth during the hydrothermal synthesis of zeolites. The increase of unit cell volume upon an increase in Al and/or Fe content(s), as indicated in Table 1, reflected isomorphous substitution of SiO_4 tetrahedra (so-called T-sites), the backbone of the zeolite

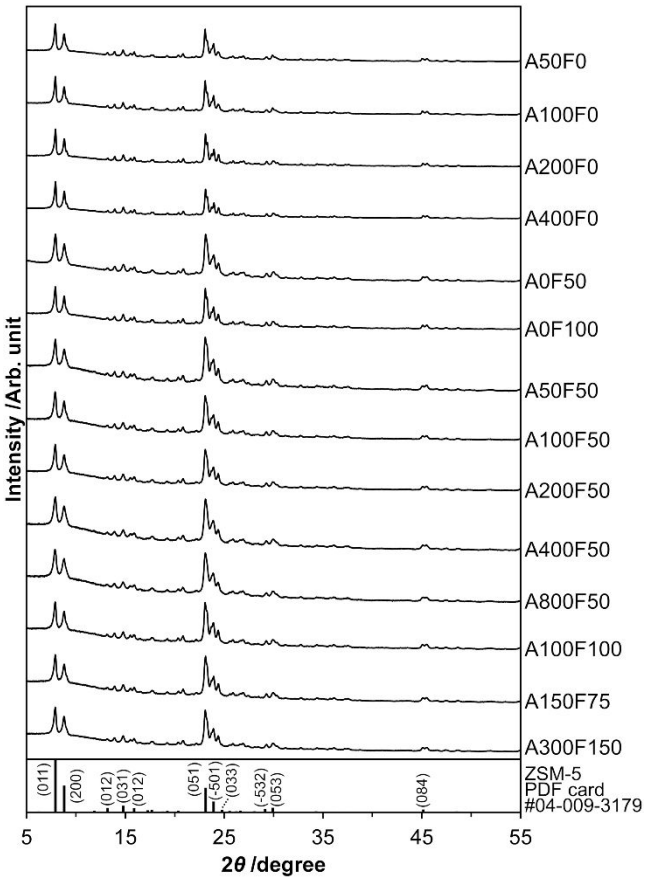

Fig. 1 XRD patterns of the synthesized MFI zeolites. All diffraction patterns were normalized by the peak height of 011 reflection at 2θ of 7.9°.[29]

framework, by AlO_4^- and/or FeO_4^- tetrahedra, due to the larger ionic radii of Al^{3+} and Fe^{3+} (0.39 Å and 0.49 Å, respectively) compared to that of Si^{4+} (0.26 Å).[33]

The N_2 physisorption isotherms for all synthesized zeolites exhibited type I behavior with an increase of N_2 uptake being observed at the relative pressure (p/p_0) of *ca.* 0.9 (Fig. S1, ESI†). These physisorption data confirmed the presence of micropores which originated from the MFI-type zeolite framework itself, in addition to mesopores derived from interparticle voids.[34] Regardless of the Al and Fe contents, the specific surface areas of the synthesized zeolites were calculated to be ≥400 $m^2\ g^{-1}$ by the Brunauer-Emmett-Teller (BET) method (Table 1), and these values are higher than the reported values for [Al, Fe]-MFI zeolites.[22,35,36] The small crystallite sizes (*vide supra*) led to an increase in the external surface area which was elucidated via the *t*-plot method (Fig. S2, ESI†).

The coordination states of the Al and Fe atoms were investigated by ^{27}Al MAS NMR and DR-UV-vis spectroscopy, respectively. Note that for the latter characterization method, although peak overlapping is typically observed and makes understanding of Fe species in a zeolite specimen complicated, this technique has been widely accepted and used to distinguish four different Fe species: tetrahedral Fe present inside a zeolite framework (200–250 nm); isolated Fe

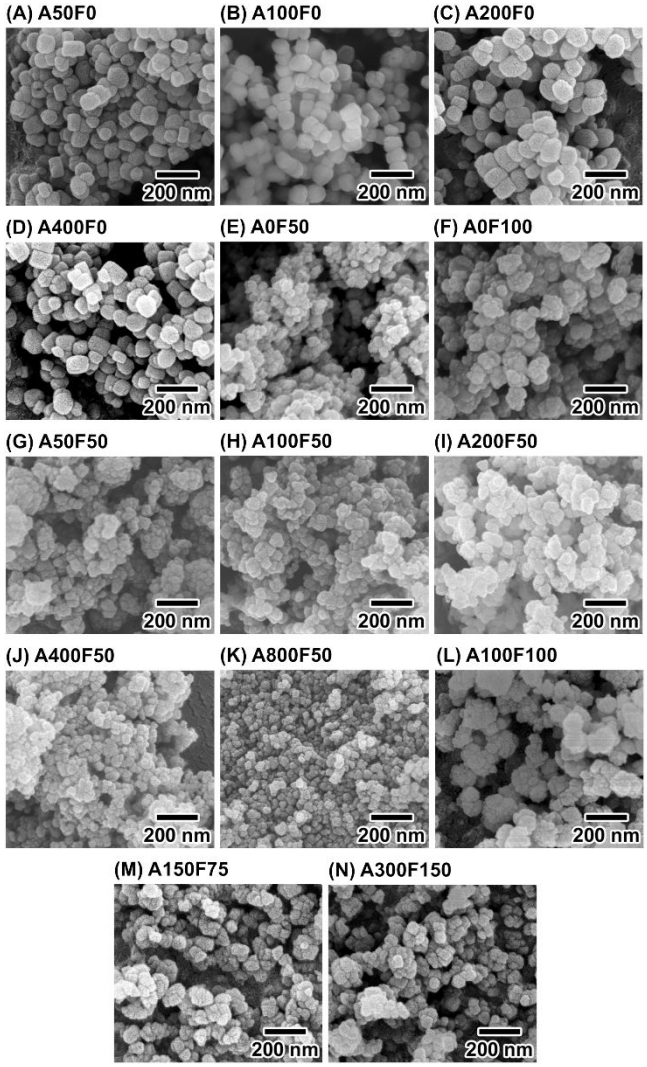

Fig. 2 Particle morphology of the synthesized MFI zeolites.

octahedra and/or Fe_xO_y clusters present outside a zeolite framework (250–350 nm); larger Fe clusters (350–450 nm); and bulk Fe oxides (>450 nm).[37–44] In the ^{27}Al MAS NMR spectra (Fig. S3, ESI†), the [Al, Fe]-MFI samples (*i.e.*, A50F50, A100F50, A200F50, and A400F50) exhibited only a prominent peak at 55 ppm which was attributed to the presence of Al^{3+} in the MFI zeolite framework,[45,46] and the intensity of this peak increased with increasing Al content. In contrast, along with the same resonance at 55 ppm, another peak at 0 ppm was observed for the [Al]-MFI zeolites with high Al contents (*i.e.*, A50F0, A100F0, and A200F0). This additional peak was derived from octahedrally-coordinated Al^{3+},[45,46] indicating that an extra-framework Al species was involved in these materials. However, the fraction of such Al species was minor, given that corresponding diffraction peaks were not observed in the XRD patterns (Fig. 1). As previously reported for the MFI-type zeolites containing both Al and Ti, the distorted structure formed by the isomorphous substitution of T-sites by the first element could generate preferential sites for the substitution by the second element;[47] this would be the reason why the peak at 0 ppm assignable to extra-framework Al species[45,46] was not observed for the [Al, Fe]-MFI zeolites. The UV-vis

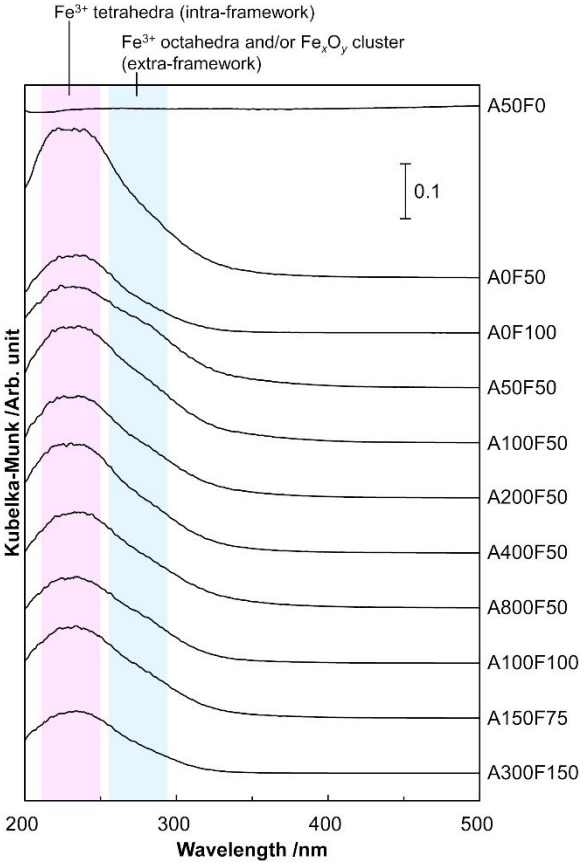

Fig. 3 Coordination state of Fe^{3+} species involved in synthesized MFI zeolites, examined by DR-UV-vis spectroscopy.

spectra for Fe-containing MFI zeolites shown in Fig. 3 gave characteristic absorption at 210–250 nm with a shoulder centered at 280 nm. Given the fact that A50F0, which is the MFI zeolite containing only Al as a substituting element, did not provide any absorption bands, the observed prominent absorption for Fe-containing MFI zeolites obviously originated from Fe species. As described above, the former peak originated from the isomorphously incorporated Fe^{3+} tetrahedra, while the latter peak is assignable to the isolated Fe^{3+} octahedra and/or Fe_xO_y clusters present in the extra-framework of zeolites as a minor species.[37–44] Notably, this shoulder peak was clearly observed for A50F50. This observation can be rationalized by lattice distortion caused by isomorphous substitution by both Al^{3+} and Fe^{3+} in high amounts, hence limiting further incorporation of large Fe^{3+} ions in the zeolite framework and resulting in the formation of extra-framework Fe species.

The density and average strength of acid sites of the synthesized zeolites were evaluated from the NH_3-TPD profiles (Fig. S4, ESI†). It should be noted that as previously demonstrated by Bagnasco, the water-vapor treatment posterior to the adsorption of NH_3 on each catalyst surface (see Experimental section) completely removed the weakly-adsorbed NH_3 species,[28] which resulted in a lack of corresponding peak at low temperature in the NH_3-TPD profiles. The NH_3-desorption temperatures for the [Fe]-MFI zeolites (*i.e.*, A0F50 and A0F100) were lower than those of the

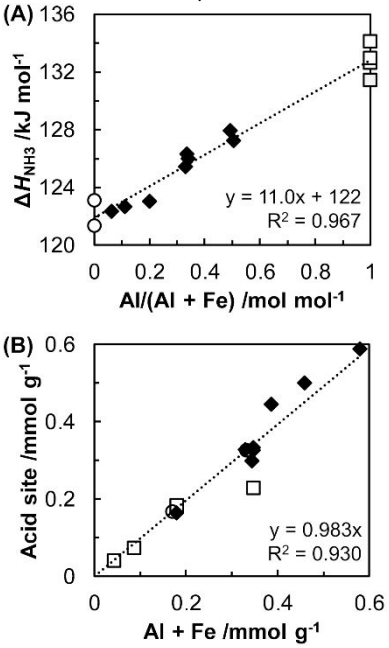

Fig. 4 Parametric plots of (A) the enthalpy change upon NH_3 desorption (ΔH_{NH3}) as a function of the proportion of Al in the total amount of Al and Fe and (B) the acid site density as a function of the total content of trivalent cations. Legends: white squares = [Al]-MFI; white circles = [Fe]-MFI; and black diamonds = [Al, Fe]-MFI.

[Al]-MFI zeolites. This order indicated that the strength of the acid sites formed over the surface of [Fe]-MFI was weaker than the cases for [Al]-MFI. As previously reported, the higher polarizability of Al provided a stronger acidity for [Al]-MFI, compared to [Fe]-MFI.[18,19] The NH_3-desorption temperatures for all [Al, Fe]-MFI samples were found to occur between those of [Al]-MFI and [Fe]-MFI, reflecting the fact that the acidity of [Al, Fe]-MFI was between that of the other two types of zeolites. For a more quantitative assessment, the enthalpy changes of NH_3 desorption (ΔH_{NH3}), which are indicators of average acidity, were examined using the method of Niwa *et al.*,[27] and the values were found to be in the range 121–134 kJ mol^{-1}, which directly correlated with the relative ratios of Al to total trivalent cations (*i.e.*, Al/(Al + Fe)), as shown in Fig. 4A. A similar linear relationship was also observed for the physical mixtures of A50F0 and A0F50 at the various mixing ratios (Fig. S5), indicating that the strong acidity of [Al]-MFI and the weak acidity of [Fe]-MFI are apparently averaged by physical mixing of multiple materials. Note that the important finding here is the linear control of the average acidity in a single material. The data plotted in Fig. 4A further indicate that, in the case of the MFI zeolites substituted by either Al or Fe, control of ΔH_{NH3} was not possible via a simple alteration of heteroatom content; indeed, even if the Si/Al ratio was varied between 50 and 400, the values of ΔH_{NH3} were in the narrow range of 131–134 kJ mol^{-1} (see the right axis of Fig. 4A). Therefore, only the co-incorporation of Al and Fe into the same framework can provide a possible means of adjusting acidity over a wide range. The DRIFT spectroscopy for the [Al, Fe]-MFI also confirmed the presence of Brønsted acid sites, given the fact that the broad absorption band observed at 3610–3630 cm^{-1}

was assignable to the stretching vibration mode of OH groups bridged by Al and Si (Fig. S6, ESI†).[48,49] The redshift of this peak

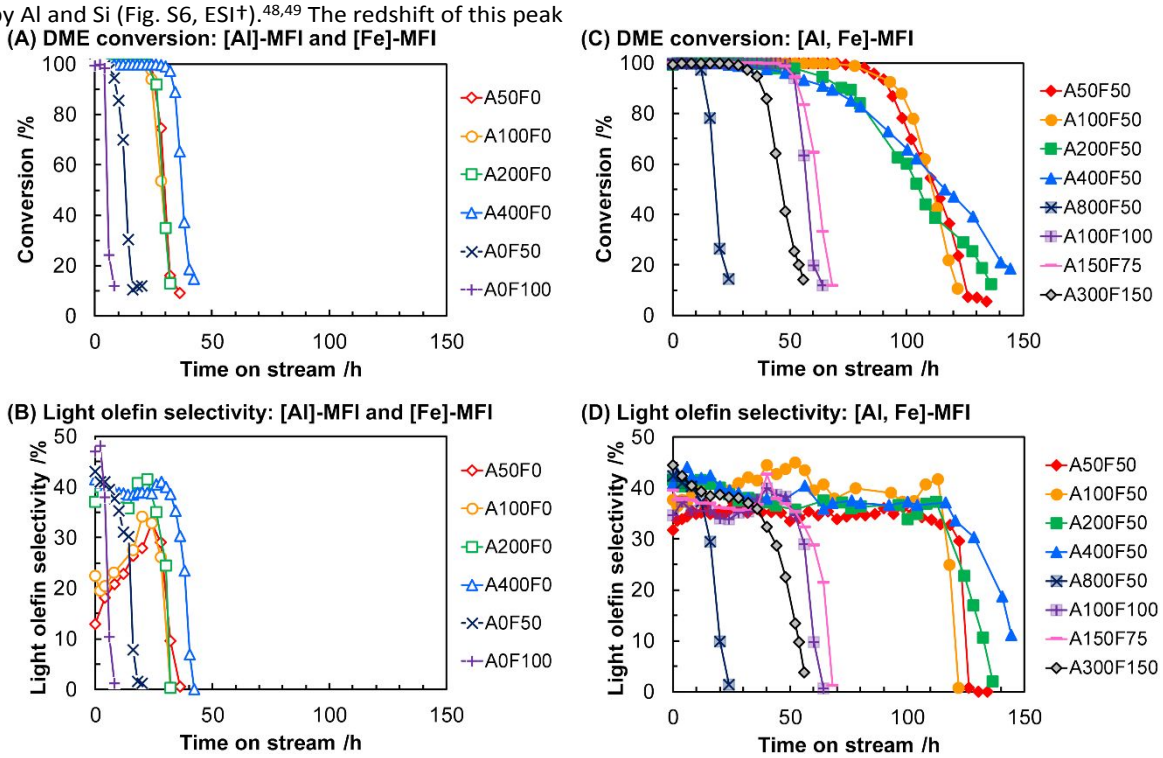

Fig. 5 Time-on-stream of the DTO reaction over the synthesized MFI catalysts. Reaction conditions: catalyst 200 mg (mixed with 840 mg of quartz sand); 450 °C; W/F = 5.8 g h mol^{-1}.

in conjunction with an increase in the Al/(Al + Fe) ratio indicated that the acidity became stronger at higher Al content, which was in good agreement with the NH_3-TPD data. Furthermore, the acid site densities were proportional to the total content of trivalent cations (Fig. 4B), indicating that each trivalent cation involved in the zeolite framework generated an acid site. Therefore, the two linear relationships found in Fig. 4 demonstrated that both the density and strength of the acid sites can be controlled linearly by simply altering the contents and relative ratios of Al and Fe.

To investigate the importance of precise control of the density and average strength of acid sites, the synthesized MFI-type zeolites were tested as catalysts for the DTO reaction, given that well-controlled and moderate acidity has been reported to facilitate this reaction in terms of catalyst lifetime;[14–17] in other words, the DTO reaction can be used as a benchmark. In this study, reaction conditions of 450 °C and a W/F of 5.8 g h mol^{-1} were applied to each experiment, to achieve >99% conversion of DME with good selectivity of the light olefins (*i.e.*, ethene, propene, and butene) and also clearly observe catalyst deactivation. Fig. 5 represents the time-on-stream (TOS) for the DTO reaction using the synthesized zeolites as catalysts (see also the detailed reaction results including selectivity of each product and carbon balance in Figs. S7–S20, ESI†). As mentioned above, all [Al]-MFI and [Fe]-MFI zeolites gave >99% conversion of DME and good selectivity of the light olefins at the beginning of the reaction (Figs. 5A and 5B), where the other by-products detected were light paraffins including methane, ethane, and propane and methanol, but the catalysts were completely deactivated (*i.e.*, formation of light olefins was not observed) within 50 h possibly due to coke deposition over the catalyst surface (*vide infra*). Under these conditions, the series of [Al]-MFI catalysts retained their activity longer than the [Fe]-MFI samples. This trend can be rationalized by the widely accepted mechanism for the DTO and MTO reactions, that is, the so-called hydrocarbon-pool mechanism, whereby the substrate molecules are initially converted to hydrocarbons (generally represented as $(CH_2)_n$) and accumulate on the surface of the catalyst and subsequently olefins are produced from the deposited hydrocarbons via a cracking reaction.[14,15,50,51] Weak acid sites are not so effective for hydrocarbon cracking, which leads to accumulation of hydrocarbons on the catalyst surface; as a result, the [Fe]-MFI catalysts lost their catalytic activity in a relatively short time. Such unfavorable function of weak acid sites for the cracking reactions also led to the high ratios of propene to ethene (*ca.* 14–15, see Table S1, ESI†). In contrast, strong acid sites promote the cracking reactions, resulting in a longer catalyst lifetime as observed for the [Al]-MFI samples with the lower ratio of propene to ethene (≤8, see Table S1, ESI†), compared to the [Fe]-MFI samples. Among the four [Al]-

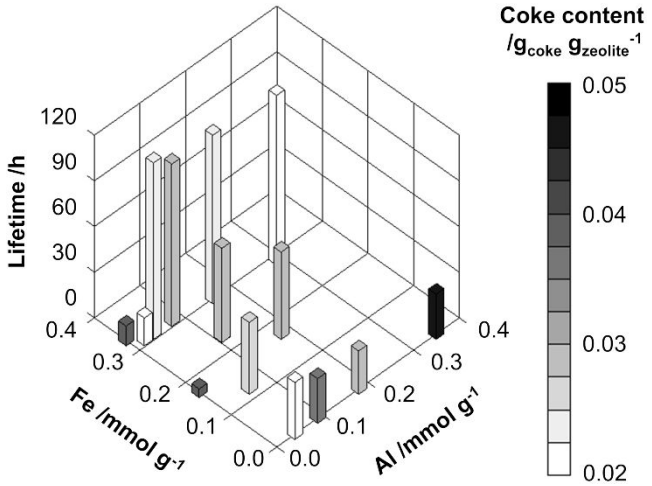

Fig. 6 Composition effects of MFI zeolites on catalyst lifetime and coke formation in the DTO reaction. Catalyst lifetime is defined as the time when the DME conversion becomes lower than 50%. The amount of coke was quantified by TGA at a TOS of 4 h, which was the shortest lifetime among all the catalysts tested. Reaction conditions: catalyst 200 mg (mixed with 840 mg of quartz sand); 450 °C; W/F = 5.8 g h mol^{-1}.

MFI catalysts, A50F0 exhibited the lowest ratio of propene to ethene because of the highest acid site density. Although such acceleration of the cracking reactions is beneficial to the extension of catalyst lifetime, strong acid sites also accelerate the hydrogen transfer of olefins to form paraffins and arenes,[14,52,53] the latter of which are successively involved in coke formation. Indeed, the [Al]-MFI catalysts with a higher Al content (*i.e.*, a larger amount of strong acid sites are involved) exhibited a shorter catalyst lifetime due to the aforementioned side reactions; as a result, among the [Al]-MFI catalysts tested in this study, A400F0 containing the lowest amount of acid sites showed the longest catalyst lifetime.

Compared to the [Al]-MFI and [Fe]-MFI zeolites, the [Al, Fe]-MFI zeolite catalysts maintained their activity, the DME conversion and the light olefin selectivity, for a longer period except in the case of A800F50, which was deactivated similarly to that of [Fe]-MFI due to its low Al content (Figs. 5C and 5D). These reaction results demonstrated that the zeolite catalysts with moderate acidity were superior in terms of catalyst lifetime to the ones with either strong or weak acidity. Among the [Al, Fe]-MFI zeolites other than A800F50, the samples with the Si/Fe ratios of ≥75 (*i.e.*, A100F100, A150F75, and A300F150) underwent complete deactivation within 70 h, while the others with the Si/Fe ratio of 50 did so later than 120 h. This difference suggests that a larger amount of Fe species provide an enhanced occasion to generate moderate acid sites, which contribute to a longer catalyst lifetime of the [Al, Fe]-MFI zeolites with the Si/Fe ratio of 50. Meanwhile, similar to the cases of [Al]-MFI and [Fe]-MFI zeolites, the [Al, Fe]-MFI catalysts with a lower Al content were prone to produce propene more selectively than ethene (Table S2, ESI†), because of the presence of relatively weak acid sites in the samples with the higher Si/Al ratio. Fig. 6 displays the effects of composition on coke formation and catalyst lifetime in the DTO reaction, the latter of which was defined as the time when the DME conversion became lower than 50%. The MFI zeolites, containing either Al or Fe, suffered from severe coke formation (see the data plotted on the axes of the basal plane of Fig. 6), which resulted in a short catalyst lifetime. In contrast, the [Al, Fe]-MFI zeolites (see the data on the basal plane, except for the ones on the axes, of Fig. 6) suppressed coke formation and exhibited a longer catalyst lifetime, implying that the moderate acidity of [Al, Fe]-MFI is key to ensuring both the progress of the desired DTO reaction and the suppression of the aforementioned side reaction that is readily catalyzed in the presence of strong acid sites.[14,52,53] Compared to a variety of reported catalysts for the DTO reaction including SAPO-34 (Table S2, ESI†),[54–64] the [Al, Fe]-MFI catalysts exhibited slightly lower selectivity of light olefins, but showed a comparable or even longer catalyst lifetime. Overall, the reaction data have clearly demonstrated that the co-incorporation of Al and Fe into the MFI framework plays a decisive role in enhancement of the catalyst lifetime for the DTO reaction. This conclusion was further reinforced by the DTO reaction using the physical mixtures of A50F0 and A0F50 at the various mixing ratios as catalysts in order to vary the Al/(Al + Fe) ratios (Fig. S21, ESI†). In all the Al/(Al + Fe) cases examined in this study, the [Al, Fe]-MFI zeolites showed at least a 3.8-fold longer catalyst lifetime compared to the corresponding physical mixtures of A50F0 and A0F50, even though the mixtures exhibited the apparent average acidities comparable to the [Al, Fe]-MFI zeolites (see Figs. 4A and S5, ESI†). In the case of the physical mixtures of A50F0 and A0F50, although it is possible for their average acidities to be apparently tuned to a moderate acidity, the actual sites with moderate acidity are not generated in these mixtures, where strong and weak acid sites are present in different particles. Consequently, once A0F50 suffers from accumulation of hydrocarbons, strong acid sites located in A50F0 particles are unable to eliminate such accumulated species via cracking reactions; thus, these physical mixtures exhibited a short lifetime for the DTO reaction. On the other hand, in the case of the [Al, Fe]-MFI zeolites, the moderate sites are generated due to the co-presence of Al and Fe in the same particles and this contributes to both the production of olefins from the hydrocarbon pool and the suppression of coke formation. Therefore, precise control of the co-incorporation of Al and Fe into the same zeolite framework is the key to ensuring well-tuned acidic properties and the desired catalytic performance.

A200F50 was further employed for the recycle test after the regeneration process at 550 °C for 6 h under air flow. As shown in Figs. S22–S24 (ESI†), interestingly, the lifetime of A200F50 was gradually increased from 107 h to 345 h upon an increase in the recycle run. The DR-UV-vis spectrum of the catalyst after the third run (Fig. S25, ESI†) indicated the formation of octahedral Fe species and/or Fe_xO_y clusters,[37–44] along with the tetrahedral Fe species present in the zeolite framework. Such sites formed during the reaction and/or the regeneration process would be responsible for the enhancement of catalyst lifetime; their detailed roles will be investigated in due course.

Conclusions

The simultaneous incorporation of Al and Fe into an MFI zeolite framework with crystallite sizes of ≤51 nm was achieved for various contents and relative ratios of Al and Fe via the combination of pre-heating and subsequent hydrothermal treatments. As demonstrated quantitatively by the NH_3-TPD measurements, control of the contents and the relative ratios of Al and Fe enabled us to linearly tune the acidic properties of the zeolites, namely, their density and average strength. In sharp contrast, the sole incorporation of either Al or Fe into the zeolite framework generated strong or weak acid sites, respectively, and was therefore not possible to control the acidity over a wide range in these cases. In the catalytic conversion of DME to light olefins, although the [Al]-MFI and [Fe]-MFI suffered from a short catalyst lifetime due to severe coke formation, the [Al, Fe]-MFI zeolites with moderate acidity suppressed coke formation and exhibited a prolonged catalyst lifetime. The results of this study have identified a means to precisely control the density and average strength of zeolites by selecting an appropriate pair of heteroatoms (*e.g.*, Al, Fe, and Ga), which undergo olation which is a key reaction for building a zeolite framework.[65,66] Such an incorporation of multiple heteroatoms and the resulting control of acidity offer an attractive opportunity to develop tailor-made zeolite catalysts with excellent activity, selectivity, and durability for selected reactions.

Conflicts of interest

There are no conflicts to declare.

Acknowledgements

This work was supported by Core Research for Evolutional Science and Technology of the Japan Science and Technology Agency (JST CREST, Grant No. JPMJCR16P3) and a Grant-in-Aid for Scientific Research (B) from the Japan Society for the Promotion of Science (JSPS KAKENHI, Grant No. 15H04181).

References

1 J. Weitkamp, *Solid State Ionics*, 2000, **131**, 175–188.
2 J. Čejka, A. Corma and S. Zones, *Zeolites and catalysis: synthesis, reactions and applications*, Wiley-VCH, Weinheim, 2010.
3 A. Corma, *Chem. Rev.*, 1997, **97**, 2373–2420.
4 A. Primo and H. Garcia, *Chem. Soc. Rev.*, 2014, **43**, 7548–7561.
5 T. Ennaert, J. Van Aelst, J. Dijkmans, R. De Clercq, W. Schutyser, M. Dusselier, D. Verboekend and B. F. Sels, *Chem. Soc. Rev.*, 2016, **45**, 584–611.
6 Y. Li, L. Li and J. Yu, *Chem*, 2017, **3**, 928–949.
7 A. Sachse and J. García-Martínez, *Chem. Mater.*, 2017, **29**, 3827–3853.
8 M. Dusselier and M. E. Davis, *Chem. Rev.*, 2018, **118**, 5265–5329.
9 J. Přech, P. Pizarro, D. P. Serrano and J. Čejka, *Chem. Soc. Rev.*, 2018, **47**, 8263–8306.
10 A. Deneyer, Q. Ke, J. Devos and M. Dusselier, *Chem. Mater.*, 2020, **32**, 4884–4919.
11 J. Wang, Y. Xu, B. Ding, Z. Chang, X. Zhang, Y. Yamauchi and K. C.-W. Wu, *Angew. Chem. Int. Ed.*, 2018, **57**, 2894–2898.
12 E. Doustkhah, J. Lin, S. Rostamnia, C. Len, R. Luque, X. Luo, Y. Bando, K. C.-W. Wu, J. Kim, Y. Yamauchi and Y. Ide, *Chem. Eur. J.*, 2019, **25**, 1614–1635.
13 R. K. Kankala, Y.-H. Han, J. Na, C.-H. Lee, Z. Sun, S.-B. Wang, T. Kimura, Y. S. Ok, Y. Yamauchi, A.-Z. Chen and K. C.-W. Wu, *Adv. Mater.*, 2020, **32**, 1907035.
14 P. Pérez-Uriarte, A. Ateka, A. G. Gayubo, T. Cordero-Lanzac, A. T. Aguayo and J. Bilbao, *Chem. Eng. J.*, 2017, **311**, 367–377.
15 P. Pérez-Uriarte, M. Gamero, A. Ateka, M. Díaz, A. T. Aguayo and J. Bilbao, *Ind. Eng. Chem. Res.*, 2016, **55**, 1513–1521.
16 Y. Hirota, M. Yamada, Y. Uchida, Y. Sakamoto, T. Yokoi and N. Nishiyama, *Micropor. Mesopor. Mater.*, 2016, **232**, 65–69.
17 K. Omata, Y. Yamazaki, Y. Watanabe, K. Kodama and M. Yamada, *Ind. Eng. Chem. Res.*, 2009, **48**, 6256–6261.
18 C. T. W. Chu and C. D. Chang, *J. Phys. Chem.*, 1985, **89**, 1569–1571.
19 A. Chatterjee, T. Iwasaki, T. Ebina and A. Miyamoto, *Micropor. Mesopor. Mater.*, 1998, **21**, 421–428.
20 Y. Yang, C. Sun, J. Du, Y. Yue, W. Hua, C. Zhang, W. Shen and H. Xu, *Catal. Commun.*, 2012, **24**, 44–47.
21 K.-Y. Lee, S.-W. Lee and S.-K. Ihm, *Ind. Eng. Chem. Res.*, 2014, **53**, 10072–10079.
22 T. Taniguchi, K. Yoneta, S. Nakaoka, Y. Nakasaka, T. Yokoi, T. Tago and T. Masuda, *Catal. Lett.*, 2016, **146**, 442–451.
23 F. C. Meunier, D. Verboekend, J.-P. Gilson, J. C. Groen and J. Pérez-Ramírez, *Micropor. Mesopor. Mater.*, 2012, **148**, 115–121.
24 D. Farrusseng and A. Tuel, *New J. Chem.*, 2016, **40**, 3933–3949.
25 L. Tosheva and V. P. Valtchev, *Chem. Mater.*, 2005, **17**, 2494–2513.
26 H. Kobayashi, M. Nakaya, K. Kanie and A. Muramatsu, *J. Environ. Sci. Eng. B*, 2015, **4**, 1–8.
27 M. Niwa, N. Katada, M. Sawa and Y. Murakami, *J. Phys. Chem.*, 1995, **99**, 8812–8816.
28 G. Bagnasco, *J. Catal.*, 1996, **159**, 249–252.
29 Database of Zeolite Structures, http://www.iza-structure.org/databases/, (accessed July 2020).
30 H. Sun, J. Wang, J. Hu and J. Zhou, *Catal. Lett.*, 2000, **69**, 245–250.
31 Q. Xiao, F. Yang, J. Zhuang, G. Qiu, Y. Zhong and W. Zhu, *Micropor. Mesopor. Mater.*, 2013, **167**, 38–43.
32 A. S. Kharitonov, V. B. Fenelonov, T. P. Voskresenskaya, N. A. Rudina, V. V. Molchanov, L. M. Plyasova and G. I. Panov, *Zeolites*, 1995, **15**, 253–258.
33 J. A. van Bokhoven and C. Lamberti, *Coord. Chem. Rev.*, 2014, **277-278**, 275–290.
34 M. Thommes, K. Kaneko, A. V. Neimark, J. P. Olivier, F. Rodriguez-Reinoso, J. Rouquerol and K. S. W. Sing, *Pure Appl. Chem.*, 2015, **87**, 1051–1069.
35 Y.-F. Chang, J. G. McCarty and Y. L. Zhang, *Catal. Lett.*, 1995, **34**, 163–177.
36 N. R. C. F. Machado, V. Calsavara, N. G. C. Astrath, A. M. Neto and M. L. Baesso, *Appl. Catal. A: Gen.*, 2006, **311**, 193–198.
37 S. Bordiga, R. Buzzoni, F. Geobaldo, C. Lamberti, E. Giamello, A. Zecchina, G. Leofanti, G. Petrini, G. Tozzola and G. Vlaic, *J. Catal.*, 1996, **158**, 486–501.
38 J. Pérez-Ramírez, *J. Catal.*, 2004, **227**, 512–522.
39 M. S. Kumar, M. Schwidder, W. Grünert and A. Brückner, *J. Catal.*, 2004, **227**, 384–397.
40 M. S. Kumar, J. Pérez-Ramírez, M. N. Debbagh, B. Smarsly, U. Bentrup and A. Brückner, *Appl. Catal. B: Environ.*, 2006, **62**, 244–254.

41 A. Zecchina, M. Rivallan, G. Berlier, C. Lamberti and G. Ricchiardi, *Phys. Chem. Chem. Phys.*, 2007, **9**, 3483–3499.
42 C. Hammond, N. Dimitratos, J. A. Lopez-Sanchez, R. L. Jenkins, G. Whiting, S. A. Kondrat, M. H. ab Rahim, M. M. Forde, A. Thetford, H. Hagen, E. E. Stangland, J. M. Moulijn, S. H. Taylor, D. J. Willock and G. J. Hutchings, *ACS Catal.*, 2013, **3**, 1835–1844.
43 K. Miyake, Y. Hirota, K. Ono, Y. Uchida, M. Miyamoto and N. Nishiyama, *New J. Chem.*, 2017, **41**, 2235–2240.
44 P. Xiao, Y. Wang, J. N. Kondo and T. Yokoi, *Appl. Catal. A: Gen.*, 2019, **579**, 159–167.
45 S. Sklenak, J. Dědeček, C. Li, B. Wichterlová, V. Gábová, M. Sierka and J. Sauer, *Phys. Chem. Chem. Phys.*, 2009, **11**, 1237–1247.
46 Q. Zhu, J. N. Kondo, T. Yokoi, T. Setoyama, M. Yamaguchi, T. Takewaki, K. Domen and T. Tatsumi, *Phys. Chem. Chem. Phys.*, 2011, **13**, 14598–14605.
47 G. Ovejero, R. van Grieken, M. A. Uguina, D. P. Serrano and J. A. Melero, *J. Mater. Chem.*, 1998, **8**, 2269–2276.
48 F. Wakabayashi, J. Kondo, A. Wada, K. Domen and C. Hirose, *J. Phys. Chem.*, 1993, **97**, 10761–10768.
49 A. Zecchina, G. Spoto and S. Bordiga, *Phys. Chem. Chem. Phys.*, 2005, **7**, 1627–1642.
50 I. M. Dahl and S. Kolboe, *J. Catal.*, 1994, **149**, 458–464.
51 S. Ilias and A. Bhan, *ACS Catal.*, 2013, **3**, 18–31.
52 S. Park, Y. Watanabe, Y. Nishita, T. Fukuoka, S. Inagaki and Y. Kubota, *J. Catal.*, 2014, **319**, 265–273.
53 S. Müller, Y. Liu, F. M. Kirchberger, M. Tonigold, M. Sanchez-Sanchez and J. A. Lercher, *J. Am. Chem. Soc.*, 2016, **138**, 15994–16003.
54 T.-S. Zhao, T. Takemoto and N. Tsubaki, *Catal. Commun.*, 2006, **7**, 647–650.
55 Y. Chen, H. Zhou, J. Zhu, Q. Zhang, Y. Wang, D. Wang and F. Wei, *Catal. Lett.*, 2008, **124**, 297–303.
56 A. Iida, R. Nakamura, K. Komura and Y. Sugi, *Chem. Lett.*, 2008, **37**, 494–495.
57 K. Omata, Y. Yamazaki, Y. Watanabe, K. Kodama and M. Yamada, *Ind. Eng. Chem. Res.*, 2009, **48**, 6256–6261.
58 S.-G. Lee, H.-S. Kim, Y.-H. Kim, E.-J. Kang, D.-H. Lee and C.-S. Park, *J. Ind. Eng. Chem.*, 2014, **20**, 61–67.
59 M. Ghavipour, R. M. Behbahani, R. B. Rostami and A. S. Lemraski, *J. Nat. Gas Sci. Eng.*, 2014, **21**, 532–539.
60 S. Park, S. Inagaki and Y. Kubota, *Catal. Today*, 2016, **265**, 218–224.
61 Q. Han, K. Enoeda, S. Inagaki and Y. Kubota, *Chem. Lett.*, 2017, **46**, 1434–1437.
62 F. Wang, Z. Wen, Z. Qin, Q. Fang, Q. Ge, Z. Li, J. Sun and G. Li, *Fuel*, 2019, **244**, 104–109.
63 S. Zhang, Z. Wen, L. Yang, C. Duan, X. Lu, Y. Song, Q. Ge and Y. Fang, *Micropor. Mesopor. Mater.*, 2019, **274**, 220–226.
64 Z. Chen, Z. Li, Y. Zhang, D. Chevella, G. Li, Y. Chen, X. Guo, J. Liu and J. Yu, *Chem. Eng. J.*, 2020, **388**, 124322.
65 J.-P. Jolivet, C. Chanéac, D. Chiche, S. Cassaignon, O. Durupthy and J. Hernandez, *C. R. Geosci.*, 2011, **343**, 113–122.
66 L. Li, W. Wei and M. Behrens, *Solid State Sci.*, 2012, **14**, 971–981.

Graphical abstract

The co-incorporation of Al and Fe at the various relative ratios into the MFI-type zeolite framework enabled to linearly control the density and strength of acid sites, and such well-tuned acidity led to a better catalyst lifetime.